Pieter Harpe
Andrea Baschirotto
Kofi A. A. Makinwa *Editors*

Biomedical Electronics, Noise Shaping ADCs, and Frequency References

Advances in Analog Circuit Design 2022

Springer

Next-Generation Molecular Detection with a CMOS Capacitive Sensor

Tim Cummins and Brian O'Farrell

Abstract CMOS biosensors hold great promise for the high volume/low-cost scalability of molecular diagnostics. However, despite many publications in this area over the past decades, mainstream consumer adoption examples are limited. This chapter explores some of these biosensor opportunities and inherent challenges. It begins with an introduction to molecular detection basics and reviews current laboratory and point-of-care detection methods. Some historical biosensor approaches and recent CMOS biosensor examples are reviewed. We present initial results of a fully synthetic SARS-CoV-2 PNA-probe assay with a standard-CMOS capacitive bead detector which aims to overcome some of the enzyme and process complexities of the previous methods.

1 Introduction

Decentralization of diagnostics and healthcare from hospitals into community care settings, and ultimately into the home, has been proposed to reduce the burden on overloaded central hospitals and laboratories. The COVID-19 pandemic and the implications for routine health maintenance during periods of nonpharmaceutical interventions, such as "lockdowns," has driven a new awareness of the value of digital health and telemedicine. This is now recognized by the World Health Organization in their 2022 *Consolidated Telemedicine Implementation guide* [1], which states: "the delivery of health-related services and information using information and communications technologies (ICTs) is a critical driver for expanding access to services and promoting continuity of care."

Modern wireless electronics and biosensors are helping to accelerate this trend, with over-the-counter home biosensors now readily available for monitoring of blood pressure, blood-glucose levels, heart rate, ECG, blood oxygen, and other

T. Cummins (✉) · B. O'Farrell
Altratech Ltd, Cork, Ireland
e-mail: tim.cummins@altratech.com

P. Harpe et al. (eds.), *Biomedical Electronics, Noise Shaping ADCs, and Frequency References*, https://doi.org/10.1007/978-3-031-28912-5_6

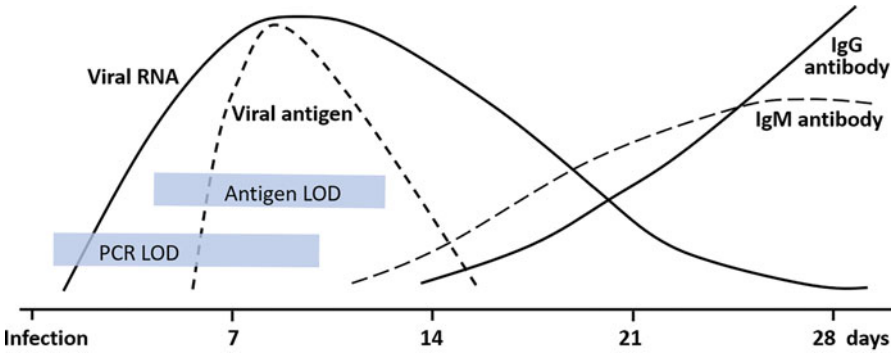

Fig. 1 Pathophysiology and timeline of viremia, antigenemia, and immune response during acute SARS-CoV-2 infection

vital signs. Regularly, these devices may not be as accurate as hospital-based diagnostics, but they nevertheless fulfil an important role in widescale screening and citizen empowerment in taking greater ownership over their own individual health journey. Use of home diagnostics, specifically, was brought to worldwide public consciousness during the recent COVID-19 pandemic, caused by the SARS-CoV-2 individuum of the species *severe acute respiratory syndrome–related coronavirus.* Lateral-flow SARS-CoV-2 rapid antigen self-test kits were found in almost every household. This was despite some initial concerns of clinicians that these were not as accurate as hospital and laboratory-based SARS-CoV-2 PCR molecular tests, or Point-of-Care LAMP SARS-CoV-2 molecular tests. Analytical sensitivity (or Limit-of-Detection, LOD) is shown for each of these in Fig. 1, which also shows the typical timelines of viral RNA, viral antigen, and antibody development in the human body following an infection. PCR is the "gold standard" test method due to its lower LOD and earlier detection of infection by detecting the actual RNA viral genome. A positive antigen test detection may not occur until a few days later, due to its higher LOD and the body's antigen response also occurring typically a few days after the viral RNA peak. Against this, subjects may test positive for SARS-CoV-2 using PCR tests long after their infectiousness is problematic, complicating clinical decisions.

The ideal for an infectious disease diagnostic would be to replicate, in a home setting, the sensitivity and specificity of laboratory DNA and RNA PCR molecular tests, but with the robustness, simplicity, and the low cost of the lateral-flow antigen test. This is illustrated conceptually in Fig. 2.

Additionally, the home test would ideally reciprocate the range of tests available in the central lab, for example, conducting both serological (antigen/antibody) tests and molecular tests (DNA/RNA).

CMOS biosensors offer great promise toward achieving this goal, with the ability to combine two key functions of biosensors: transducing and signal processing.

On the other hand, Hassibi [2] notes that CMOS biosensors require complex and upfront capital-intensive manufacturing/assembly processes and convergence

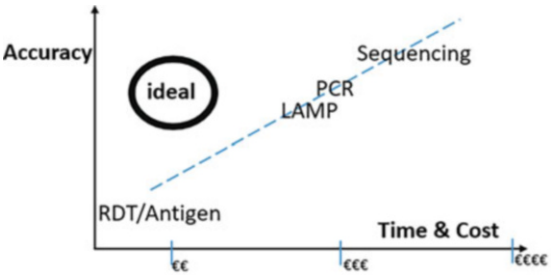

Fig. 2 Simplified representation of test accuracy versus time and cost

of multiple disciplines beyond engineering. He cautions that CMOS biochips are "an overpromised field with lots of unproven technologies and failed projects, and limited successful commercial products."

In this chapter, we delve into some of the possible reasons for this and review some recent biosensor and CMOS biochip examples. We conclude the chapter with initial results for a new approach, employing a CMOS fringe-field bead capacitance sensor, fabricated on a standard CMOS process, where the bead is a proxy for a DNA or RNA molecule captured in the upstream assay by peptide nucleic acid (PNA) probes.

2 Molecular Detection Methods

Optical microscopy of micrometer cells and bacteria has been in existence since the 1600s. However, the nanometer dimensions of DNA, RNA, and antibody/antigen proteins mandate the use of electron microscopy or X-ray crystallography in research laboratories to identify and observe them directly (Fig. 3). In this section, we review the medical diagnostic methods which have emerged in recent decades of detecting and identifying these proteins and molecules, directly and indirectly.

2.1 Antigen and Antibody Lateral Flow Devices

Lateral flow device (LFD) immunoassays are common, user-friendly, inexpensive, and readily available testing devices that are used for detection of analytes, directly or indirectly, to aid in diagnosis of medical conditions. Direct detection of human chorionic gonadotropin (HCG) hormone in the home pregnancy test is perhaps the most well-known example. Although over 50 years old, LFDs nonetheless proved a most valuable technology during the recent COVID-19 pandemic, indirectly detecting SARS-CoV-2 positivity by detecting the body's antigenic response to the virus. They are also called rapid-diagnostic tests (RDT), giving a result usually within 15 to 30 minutes. A derivation of classical chromatography, they work by binding specific antibodies conjugated to nanoparticles with a specific target in

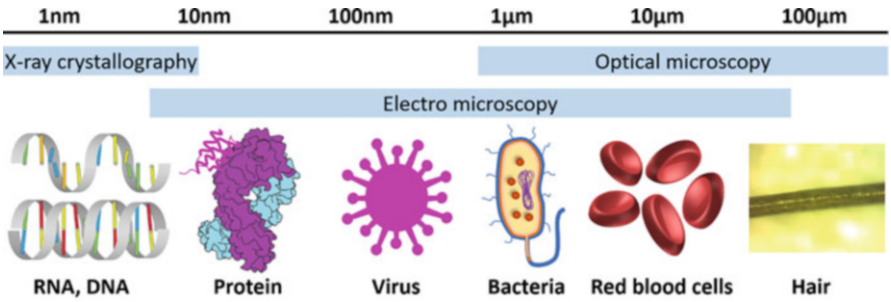

Fig. 3 Relative molecular dimensions of various biological structures

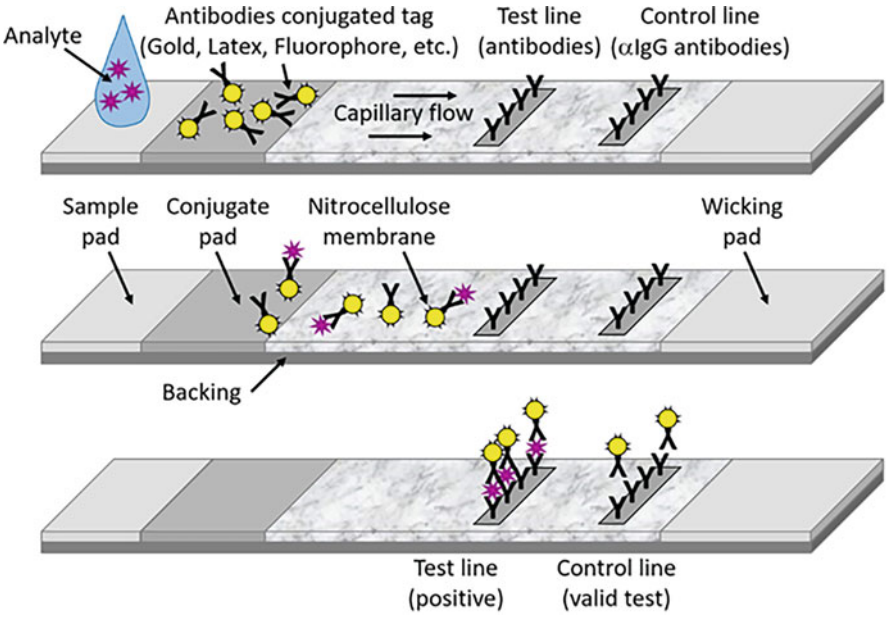

Fig. 4 Lateral flow assay architecture

the sample. In the case of SARS-CoV-2, this is an antigen target. This antibody-antigen complex moves via capillary flow to a test area. Where an antigen is bound, the complexes become captured on another antibody, which forms a sandwich across the antigen, holding the complex in place and indicating a positive test. A control line downstream captures nanoparticles with no antigen attached through interactions with the initial antibody. The control and positive lines are identified by the presence of a colored line due to bead-labelling (Fig. 4). The reader is referred to reference [3], which gives a detailed description of LFD types and methods of operation.

2.2 DNA Sequencing

Sequencing is the process of determining the nucleic-acid sequence – the order of nucleotides – of the five standard nucleobases, the fundamental units of the genetic code of all living matter: adenine (A), cytosine (C), guanine (G), thymine (G), and uracil (U). The bases A, G, C, and T are found in DNA, while A, G, C, and U are found in RNA (Fig. 5). Note the binding or hybridizing patterns: A-T and C-G, that is, adenine always binds to thymine, and cytosine always binds to guanine. This is important for probe and primer design in molecular tests.

The reader is referred to reference [4] for an overview of sequencing methods and technologies.

Knowledge of DNA sequences has become indispensable for basic biological research, medical diagnosis, and virology. However, sequencing is available only in advanced university and hospital research facilities, or in very few central virus-reference laboratories. Despite much optimism over the years, it remains a stubbornly expensive method, ranging from hundreds (e.g., for short-reads or single gene) to thousands of dollars for full-genome sequences, for example, in cancer analysis [5]. The cost variation is largely explained by complicated molecular biology upstream, which can be used across samples to maximize the output of a sequencing run. This works by applying sequence tags, which function as a code, which can later flag to bioinformaticians which sequences came from which sample. This lowers the cost per sample but at the considerable cost of extra processing, which again requires a sophisticated central laboratory.

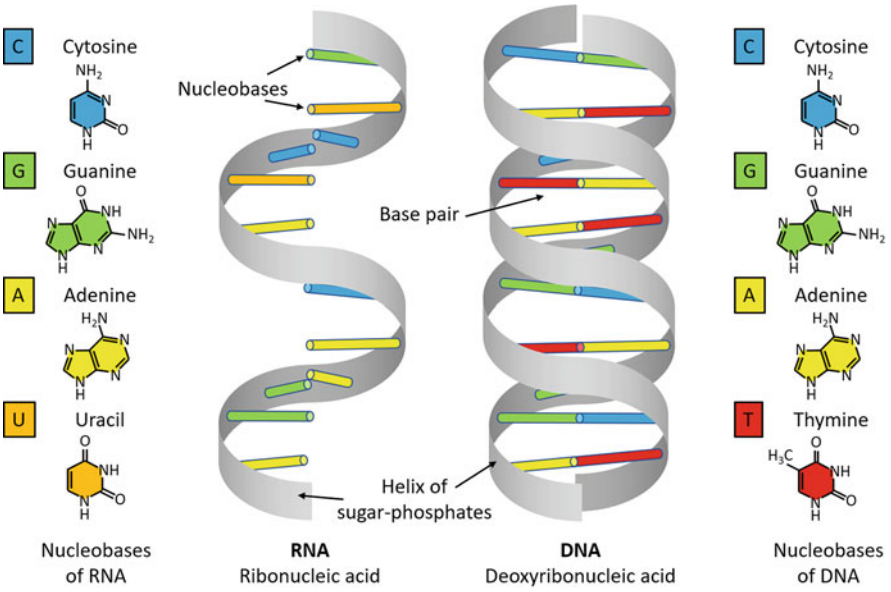

Fig. 5 Nucleobase structures of double-stranded DNA and single-stranded RNA

Sequencing became very important in late 2019, at the start of the COVID-19 pandemic, in identifying the causative novel coronavirus (nCOV). This showed it as a novel strain of the *severe acute respiratory syndrome* virus. Sequencing enabled the rapid availability of the genome of the causative agent to researchers and diagnostic vendors. Due to its resulting severe acute respiratory symptoms, it became known as SARS-CoV-2. A viral particle of approx. 100 nm diameter, its first complete sequence, known as the "Wuhan reference genome," was uploaded to the public GenBank database (accession number NC_045512) in December 2019 [6]. This was a new individuum of *severe acute respiratory syndrome–related coronavirus* which had earlier caused the SARS epidemic. This information allowed researchers and biopharma companies to quickly assess available diagnostic and vaccine technologies designed for related coronaviruses. An RT-PCR test was provided to the WHO by January 14, 2020 (Corman et al. [7]).

The SARS-CoV-2 structure is shown in Fig. 6, and an expanded portion of its sequence is shown in Fig. 7.

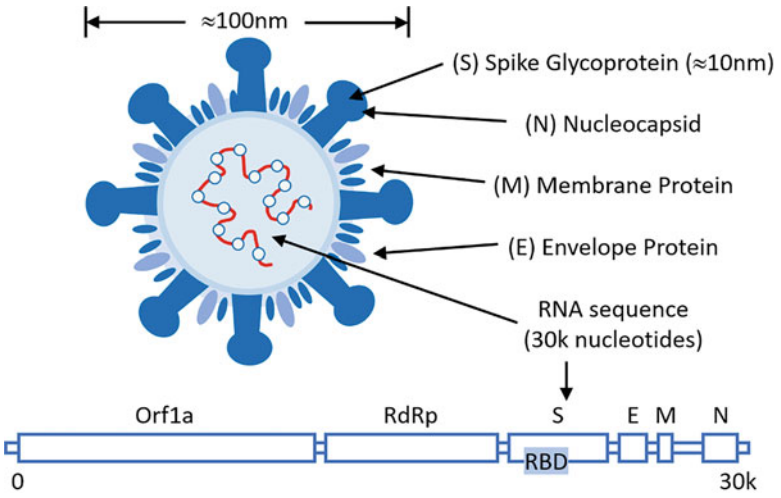

Fig. 6 The SARS-CoV-2 viral particle structure (Based on [8])

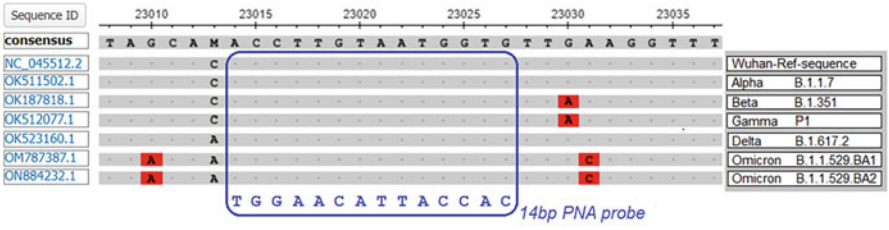

Fig. 7 Portion of the SARS-CoV-2 spike gene receptor binding domain (RBD), showing some mutations, and a PNA probe targeting a region conserved across many variants

2.3 PCR Testing

The polymerase-chain-reaction (PCR) method gets its name from the amplification of a target DNA or RNA sequence into billions of copies. This is enabled by the heat-resistant enzyme *Taq* DNA polymerase, which was first discovered in a thermophilic bacterium *(Thermus aquaticus)* living successfully in boiling geyser waters in Yellowstone National Park [9]. Theoretically, a single copy of the target DNA or RNA could be amplified and detected. This form of low copy number PCR is traditionally common in forensics but was problematic as that level of sensitivity could be caused by very incidental or even historic contact with evidence in a case. It can also cause problems where detection of DNA or RNA is reflective of past rather than current infection. In practice, however, the LOD of commercial PCR tests ranges from a few dozen to several hundred copies/mL, and even thousands of cp/mL for some highly mutated viruses. This lesser sensitivity commonly reflects inefficiency in the many steps during sample processing and/or inefficiencies during the many cycles of PCR, explained further below.

PCR can be employed for detection once the DNA or RNA sequence of a target virus or pathogen is already known. This allows design of combinations of short sequence-specific probes which target the DNA or RNA sequence and allow subsequent enzymatic processing events to occur allowing a detectable reaction.

A target DNA sequence can be detected by first breaking apart the double-stranded DNA in the sample ("denaturing") to single strands, usually at high temperature, for example, 95 °C. This makes available the single-stranded sequences for probing by chemically synthesized complementary probes or primers which target specific regions of the target sequence.

PCR probes are typically >25 nucleotides or base pairs (nt or bp) in length. However, for illustrative purposes, an 8-bp example (c) is given below. If the complementary probe sequence (c) and target sequence (b) match, they should bind with 100% specificity. If even only one nucleobase has mutated, as in (a), then they should not match and not bind to each other. This single-based mutation (SBM) is also known as a single-nucleotide-polymorphism (SNP). Good "SBM specificity" is a key measure of a good molecular test:

(a) A**G**TTCCGG – a SNP or SBM mutation which should not match.
(b) AATTCCGG – The 'target' sequence to match/bind and be detected.
(c) TTAAGGCC – Complementary probe/primer sequence to detect the target.

Figure 8 shows the first two cycles of a PCR reaction. The target DNA is denatured (at ~95 °C typically), that is, it is split into two separate strands. In the annealing step (45 °C to 60 °C), the two primer probes "match," that is, bind or hybridize to the target region. Then the temperature is raised (from ≈72 °C to 75 °C), and the polymerase enzymes then promote double-stranded extension of the sequence. This results in two double-stranded copies of the original target sequence portion. The denature-anneal-extend temperature cycle then repeats, creating four copies, as shown in Fig. 8.

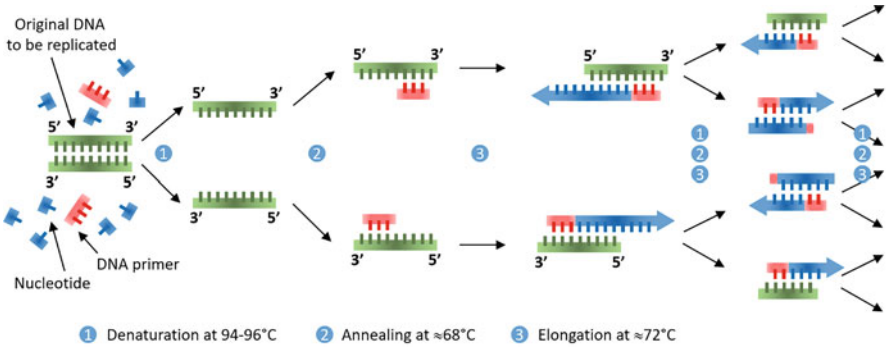

Fig. 8 PCR (polymerase chain reaction) cycles

Each further temperature cycle therefore doubles the number of copies. Thus, 30 temperature cycles will create 2^{30} or 1 billion copies from the original short target region. If the probes are labelled with a fluorescent dye marker, then the billion fluorophores create a faint glow, which is detected by an optical scanner or plate reader. A single PCR reaction will typically have three or four nonoverlapping fluorophore dye colors, enabling detection of two DNA targets and a positive and negative control. Higher multiplex testing of many targets is possible by splitting the sample into different wells or channels in more complex laboratory instruments. However, this adds complexity and makes the technology even less suitable for decentralization to point-of-care and home settings.

These PCR laboratory instruments typically have a four-figure to six-figure cost, and the PCR cost per test remains high, often $100+, or perhaps lower in certain high-throughput situations [10]. The PCR equipment costs reflect the complexity of heating/cooling with Peltier cells, chambers, valves, actuators, and bulky laser optical detection systems comprising photomultiplier tubes, filters, lenses, and array illumination for 96-well or 384-well multiplex plates. The per-test costs reflect the significant overheads of trained specialist staff required to run the tests, as well as extensive laboratory infrastructure of air conditioning, isolation fume hoods, centrifuges, and other sample preparation equipment and reagents, together with refrigerators and freezers for storing these. The pre-PCR sample preparation stages of filtration/centrifuging, separation, lysing, DNA extraction (e.g., with magnetic beads), and purification are quite complex. Many of the errors in PCR testing occur during the pre-PCR sample preparation phase. Agencies like FindDx have negotiated lower (four-figure) equipment and per-test costs for HIV and TB viral tests in low- and medium-income countries, in conjunction with donor body subsidies [11]. However, trained staff are still required for sample preparation, extraction, and pipetting. This inhibits true widescale community deployment.

An interesting development during the COVID-19 pandemic was the Emergency Use Authorization (EUA) for Visby Medical's SARS-CoV-2 portable test [12].

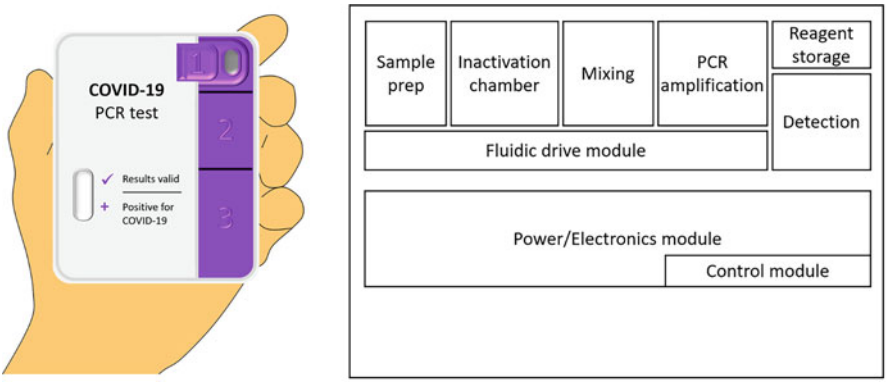

Fig. 9 Visby Medical SARS-CoV-2 "PCR in the palm of your hand". (Based on https://www.visbymedical.com/covid-19-test/ and [13])

It miniaturizes and integrates the entire sample-handling, thermocycling, and detection process, into "PCR in the palm of your hand", as shown in Fig. 9:

Its lower limit of detection is 1112 copies/mL [14]. It is currently priced at $155 for a single-use disposable test [15].

2.4 LAMP/Isothermal Testing

Loop-mediated isothermal amplification (LAMP) has emerged as an alternative to PCR in recent years. It also uses polymerase enzymes for replication and amplification of the target DNA. However, there is no temperature cycling, which simplifies the equipment required. Instead, it requires six primer probes for specificity (typically >50 bp) and employs a single ("isothermal") temperature (60 °C typically) to promote the enzymatic amplification reaction. Reference [16] provides a more detailed explanation and review of LAMP diagnostics.

Because of their simpler equipment and operation, LAMP tests are becoming prevalent in point-of-care settings, for example, the Abbott IDnow system. However, its LOD (3900 to 20,000 cp/mL) [17] is not as sensitive as PCR. Critically, the colorimetric detection principle used with some LAMP assays is very sensitive to sample pH which was found to be a barrier to LAMP during the pandemic. The large numbers of probes involved in LAMP may also cause more problems compared to PCR, when variants and sub-variants mutate creating novel mismatches to probes designed for the original wild-type genome. Multiplexing for variant level detection or for ruling in or out other viruses with similar symptoms is also more complicated due to problems with the LAMP probes interfering with each other.

Cue Health received an EUA for their isothermal amplification single-plex SARS-CoV-2 home test during the COVID-19 pandemic [18]. It has a palm-sized

heater/reader unit ($159), a single-use cartridge and swab with a per-test cost of $52 [19], and an LOD of 1300 copies/mL [20]. For detection it employs a biosensor, where electrochemical labels are used to generate a nano-amp detection current as amplicons are generated and bind to capture probes anchored on electrodes.

3 Biosensors

Biosensors offer good promise toward reducing the size and cost of diagnostic systems. Biosensors combine a physicochemical detector (often an electronic device) with a biological component, which allows a specific chemical or biological analyte to be detected. Frequently such biosensors feature a self-assembled monolayer (SAM) where the biological component has been attached to the surface of the sensor. Lei at al [21] list many published research examples of biosensor transducers (gold electrodes, ISFET, photodetector, cantilever, nanowire, hall-sensor, SAW, spiral coil, silicon nanowire) and the various sensing parameters employed in these (magnetism, fluorescence, mass, nuclear-spin, charge, capacitance, impedance, and current-voltage cyclic-voltammetry). In this section, we focus on electrical biosensors.

3.1 Electrochemical Glucose Sensor

The best-known and most commercially successful biosensor is the blood-glucose electrochemical biosensor (Fig. 10). It consists of a reader with control electronics, and single-use disposable test strips, for manufacturability in high volume and at low cost. Its working principle, perfected over many decades, is to immobilize glucose oxidase enzyme on a working electrode. The enzyme catalyzes the conversion of glucose in the blood sample to gluconic acid and hydrogen peroxide (H_2O_2). Glucose is quantified by the electrochemical measurement of the H_2O_2, either by current-flow amperometry or cyclic voltammetry (CV, sweeping of the working-electrode voltage versus the reference-electrode voltage with DACs).

Known as a potentiostat, the working principle and typical CV circuit is shown Fig. 11. A silver-chloride reference electrode (RE) holds the assay liquid at a fixed potential. The voltage on the working electrode (WE) is then varied with respect to RE, resulting in an analyte-indicative current flow in the counter electrode (CE).

Less invasive versions of the glucose sensor have recently been approved in the market, for example, the Abbott Libre arm-mounted sensor (Fig. 12). This has a subcutaneous electrochemical sensor on the tip of a 5 mm plastic filament, a 0.1mm^2 carbon working-electrode, a carbon counter electrode, and an Ag/AgCl reference electrode. The PCB has a thermistor to measure body temperature, a battery, and a single-chip microcontroller. This has analog-to-digital (A-to-D) converters and I-V amplifiers to measure glycemia amperometrically, nonvolatile memory for

Fig. 10 Blood glucose biosensor reader and test strip

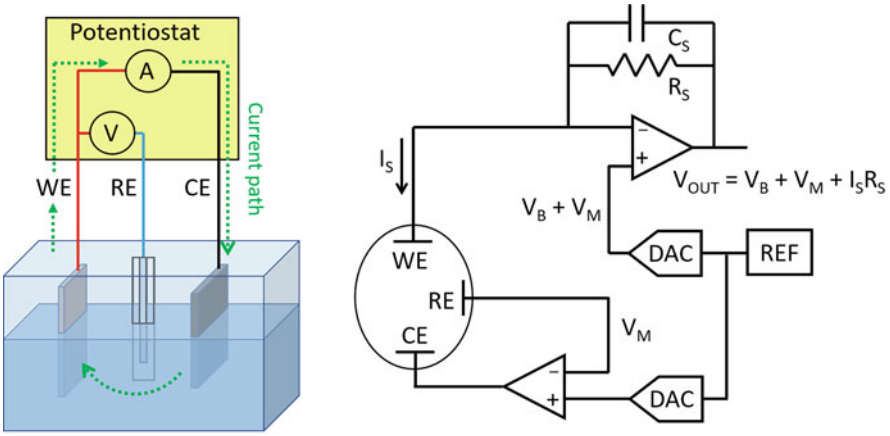

Fig. 11 Electrochemical sensor working principle (left) and potentiostat control circuitry (right, based on www.analog.com)

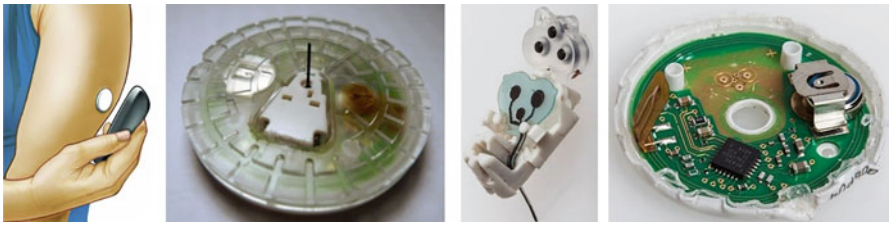

Fig. 12 Libre arm-mounted sensor, sensor tip, and internal PCB

calibration, and an NFC radio to communicate with a nearby smartphone for results tracking and uploading to a clinician if enabled.

Due to electrode wear and drift, it is recommended for only 2 weeks of operation, then to be replaced with a new sensor. This is an excellent example of sensor, electronics, and clinical communities bringing telemedicine and remote health management into everyday use. Despite the potential risk of not being as accurate as a finger-pick blood-glucose sensor reading, patients and users have readily adopted this arm sensor for its sheer convenience and comfort factors.

Of note, there has been a drive amongst the diabetic community to "hack" the Libre sensor employing online tutorials to extend its lifetime to 28 days or longer [22] and recalibrate it every few days with a finger-pick blood glucose reading.

3.2 Electrochemical DNA Sensor

DNA is a negatively charged conductive molecule, reminiscent of an electric wire. Barton, Kayyem, and others at California Institute of Technology in 1992 began using this property to detect a target DNA by immobilizing complementary DNA probes on electrodes [23]. These are usually noncorroding gold electrodes for assay stability and reliability. When the DNA target binds to the capture probe, the resulting H^+ ions released are detected by electron flow in the electrode. There are many variations, for example, the labelling of the probe with an Fe^+ ferrocene molecule. Cyclic voltammetry sweeps of the electrode voltage then cause reduction-oxidation of the ferrocene, with resulting change of current flow through the DNA (Fig. 13).

Just like the glucose sensor, electrochemical DNA sensors also took decades to reach large-scale commercialization. For example, Kayyem branded his developments as eSensor® and spun it out as Clinical Micro Sensors in 1995. This was acquired by Motorola in 1999, divested to Osmetech in 2005, rebranded to GenMark-Diagnostics for IPO in 2010, and acquired by Roche in 2021.

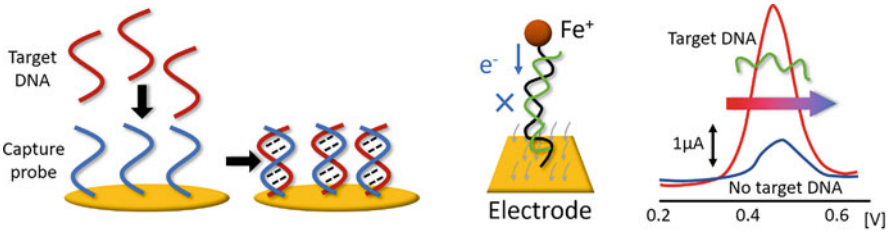

Fig. 13 Electrochemical DNA detection sensor principle

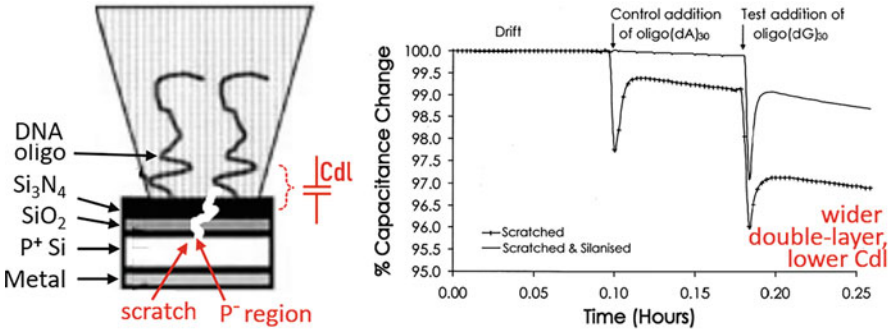

Fig. 14 Capacitive DNA sensing principle (From [23], with notes added)

3.3 Capacitive DNA Biosensors

In 1998, Berggren et al. demonstrated capacitive DNA detection with attomolar sensitivity of immobilized DNA probes on gold rods with a self-assembled monolayer (SAM) of oligonucleotides [24]. The detection principle relies on DNA being a negatively charged molecule. This repels anions in the surrounding electrolyte. When immobilized on a surface, a further layer of ions agglomerates at the surface (Helmholtz/Stern layer). This results in a double-layer (Debye layer) charge-depletion zone (similar to a P-N junction depletion region). Typically, a few nanometers wide, it has a capacitance C_{dl} ranging from pF to nF per cm^2.

Nano-rods, nano-pillars, and carbon-nanotubes for DNA detection have also been patented and published, leveraging the high surface-to-volume ratio of these structures for sensitivity. However, these structures are difficult to manufacture in high volume. Few, if any, of these have been commercialized.

Berney et al. in 2000 demonstrated capacitive DNA detection on a planar P^+ doped silicon substrate with an oxynitride passivation surface [25]. Figure 14 shows its C_{dl} reducing as DNA is added/immobilized, due to the double-layer being widened as the negatively charged DNA repels anions in the surrounding liquid.

Figure 14 also shows higher sensitivity being achieved by scratching the sensor surface. Berney attributes this to a lightly doped P^- region being formed by the scratch. Just like a lightly doped P-N junction, this results in further widening of the charge-depletion region and even more reduction in C_{dl}. The limit of detection achieved is 100 pmol.

3.4 Magnetic Bead GMR Biosensor

Paramagnetic beads are used in many molecular biology assays, for example, in DNA and RNA extraction, purification, and labelling. They are magnetic only in the

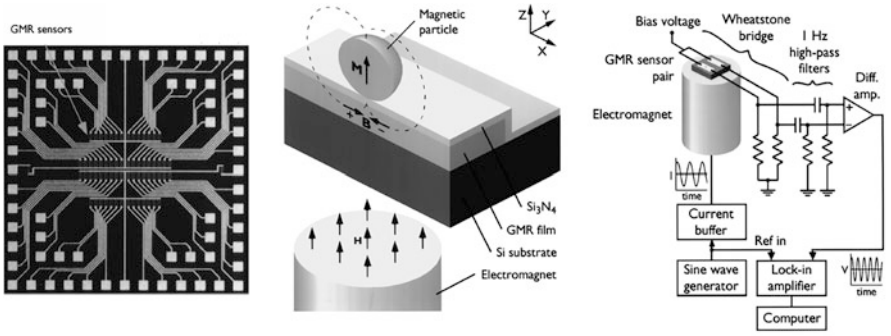

Fig. 15 Magnetic bead GMR biosensor (From [24])

presence of a magnetic field and lose their magnetism when the field is removed. This prevents agglomeration and clumping effects, which could interfere with the assay. Their diameters range from a few tens of nanometers to a few microns. Different surface coatings, chemistries, or capture probes give each type of bead its own binding properties. The bead, with a captured DNA or RNA target attached, can be removed from the lysed sample by an external magnetic field and moved through further wash and purification steps.

The concept of using the large paramagnetic bead itself as a "label" for detecting its captured DNA has been proposed, for example, Baselt et al. in 1998 with a giant magneto resistor (GMR) biosensor [26]. This has two identical GMR sensors, operating at 2.5 mA each, configured in a Wheatstone bridge detection circuit, as shown in Fig. 15. The operating principle is to detect a small differential variation of GMR sensor resistance in response to a magnetic field change due to the presence of a bead on one sensor. A downside is the requirement for a large external magnet to create the magnetizing field. This negates some of the advantage of miniaturizing the sensor itself.

4 CMOS Biosensors

The NPN base-emitter ΔV_{be} temperature sensor (Widlar 1965, [27]) and the ISFET pH sensor (Bergveld 1970, [28]) are among the earliest examples of semiconductor sensors. In both cases, it took years or decades of co-integration of signal-conditioning, calibration, and digital readout circuits for these to reach high-volume commercial success. In this section, we look at the ISFET, and some other CMOS biosensor examples, and discuss their commercialization journeys.

4.1 The ISFET

The basic structure of the ISFET (Ion-Sensitive Field-Effect Transistor) is shown in Fig. 16 (L). It is similar to a standard MOSFET, except it has liquid over the gate area. This liquid is held at a fixed voltage by an immersed reference electrode, typically of silver-chloride construction. In this example, the reference electrode is tied to the source voltage ($V_{GS} = 0$ V). The basic principle is that pH changes in the liquid alter the charge in the gate region. The effect appears as a modulation of the threshold voltage, of approximately 50 mV/pH. This causes changes in drain-source current, as shown in Fig. 16(R):

- I_{ds} = max for low pH of 2, when H^+ ions in the liquid are a maximum
- I_{ds} = min for high pH (10), when H^+ ions in the liquid are a minimum

The reader is referred Bergveld's 2003 paper "30 years of ISFETOLOGY" [29], which is an interesting and even sometimes wistful look back at the ISFET's commercialization history – or lack thereof. Despite hundreds of published ISFET papers over the decades and over 100 patents granted to various inventors, it achieved only small-scale commercialization in a few niche areas. It did not see adoption in the biomedical applications initially envisioned, due to a variety of biocompatibility, packaging, and repeatability issues, including reference electrode reliability. It also had difficulty competing against "cheap and cheerful" paper-strip and glass pH sensors. He notes the integration of an ISFET in a CMOS process in 1999 [30], and discusses the issues and obstacles which universities, innovators, and small-companies face in further development, such as finding grant-support for an "old" technology, or whether it needed "big-players" and large "market-pull" applications to justify further investments. He concludes his 2003 paper with thoughts on what may or may not happen in "possibilities for the next 30 years."

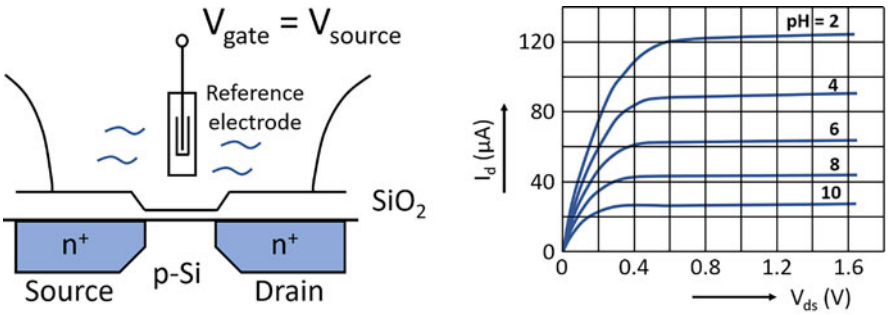

Fig. 16 (L) ISFET structure, and (R) I_d-vs-pH (with $V_{gs} = 0$ V) (Based on [29])

4.2 ISFET DNA Detection and Ion Semiconductor Sequencing

A few years later, DNA detection and sequencing emerged as big "market-pull" applications, with ISFET detection of the hydrogen ions generated during DNA polymerization, that is, the hybridizing of a single-stranded DNA with its complementary probe sequence. In 2004, for example, Toumazou patented readout circuits for CMOS ISFETs [31], culminating in a 19-SNP DNA detection chip presented at ISSCC 2010 [32] (Fig. 17).

In 2003, Hassibi et al. proposed DNA polymerization and H^+ ion-generation as a method of DNA sequencing [33]. Known as "ion-semiconductor-sequencing" and "sequencing by synthesis," the unknown target DNA sequence is determined by the detection of the hydrogen ions that are released when a complementary strand is extended based on the sequence of a template strand.

In 2007, Ion Torrent Inc., based on the work of Toumazou, Hassibi, and others, took this concept further by integrating over one million ISFETs on a CMOS chip (ION 314) [34]. Each ISFET has its own microwell with its own unique template strand, from a large library of strands covering large parts of the DNA genome to be identified. Other chips followed, with many more ISFETs to enable sequencing of longer genomes, for example, ION 316 (6.2 M ISFETs) and ION 318 (11.1 M ISFETs) for 10^8 and 10^9 bases sequenced, respectively.

The multi-ISFET and microwell principle is illustrated in Fig. 18 (Huang [35]):

Figure 19 shows Huang's implementation of a high-speed 12-bit pipelined A-to-D converter for detection of the multiple ISFET H^+-induced currents, via row and column decoders, sample-hold, and pre-amplifiers.

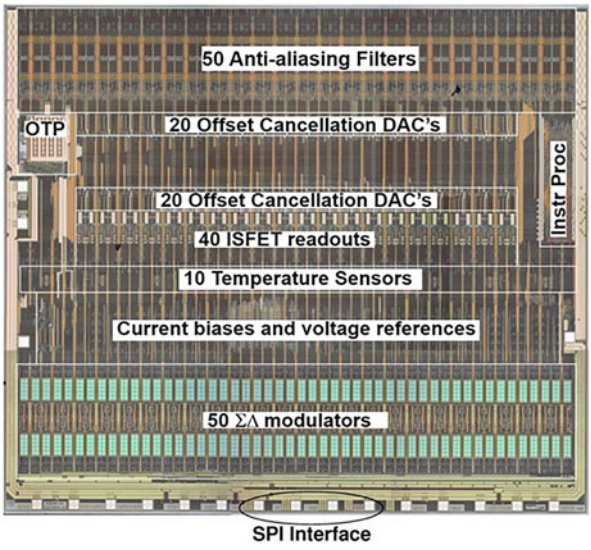

Fig. 17 0.35 μm CMOS chip, 5.5 × 4.7 mm, with 40 ISFETs, for DNA 19-SNP detection (From Ref. [32])

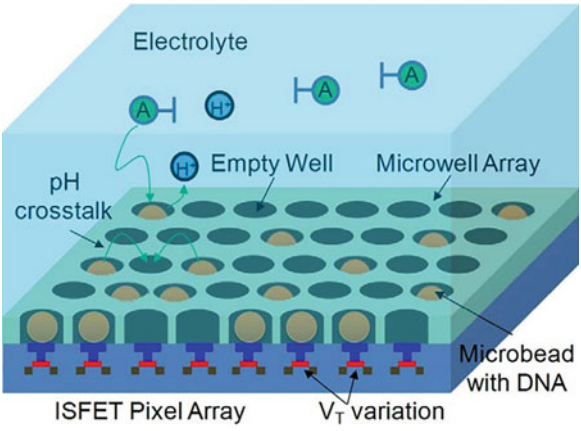

Fig. 18 CMOS multi-ISFET/microwell/microbead chip for DNA sequencing (From [35])

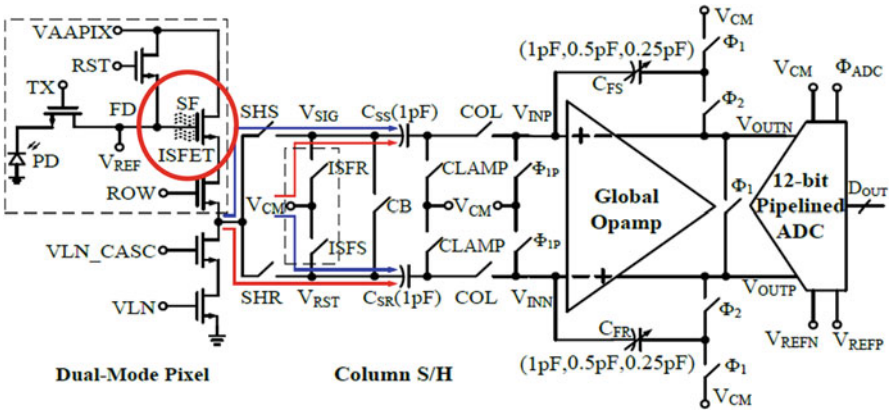

Fig. 19 Multi-ISFET H+ detection, amplification, and conversion circuits (From [35])

4.3 CMOS Hall Sensor Biochip

Boser and Florescu addressed bead detection on a CMOS biochip by integrating a microcoil to generate the magnetizing field and an N-well Hall sensor for bead detection in a fully integrated solution that required no external magnets [36]. Figure 20 (L) shows the microcoil Hall sensor arrangement, and (R) the CMOS process modifications required: aluminum wet etching, RIE dry plasma trench etching to optimize bead location on the sensors, and CR/Au deposition for gold-coating to allow protein adsorption for assay specificity. Figure 21 shows an enzyme-linked immunosorbent assay (ELISA) sandwich assay conducted atop the biosensor. The gold-surface is first coated with surface antibodies and polyclonal goat IgG specific to the F_{ab} region of Human IgG. Human IfG antigen is then introduced and incubated. A successful binding event results in the magnetic bead being captured atop the Hall sensor and detected, its large mass providing a form

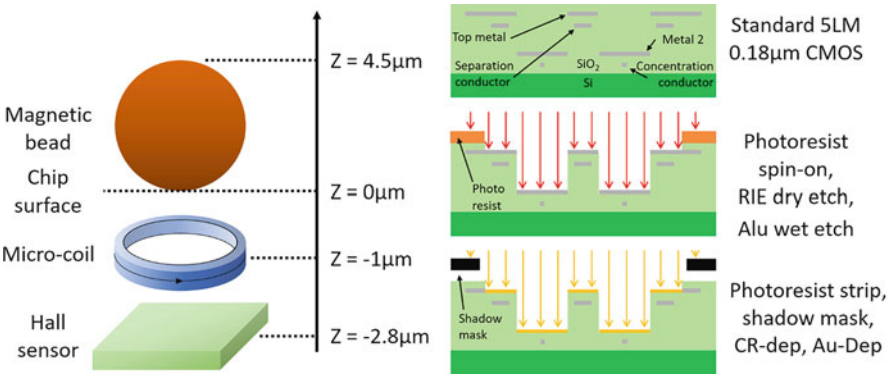

Fig. 20 (L): Microcoil and Hall sensor; (R): CMOS process modifications (Based on [36])

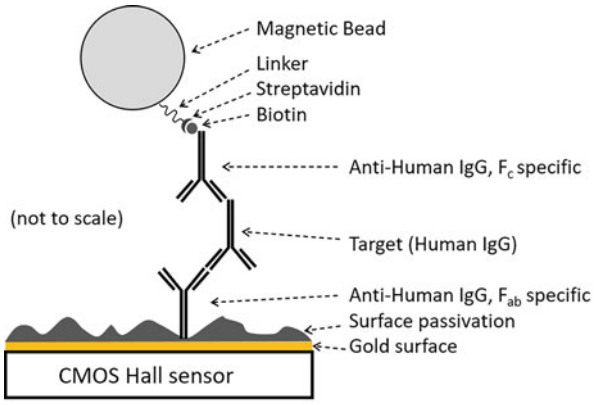

Fig. 21 ELISA-type assay conducted on the surface of the Hall sensor (Based on [36]])

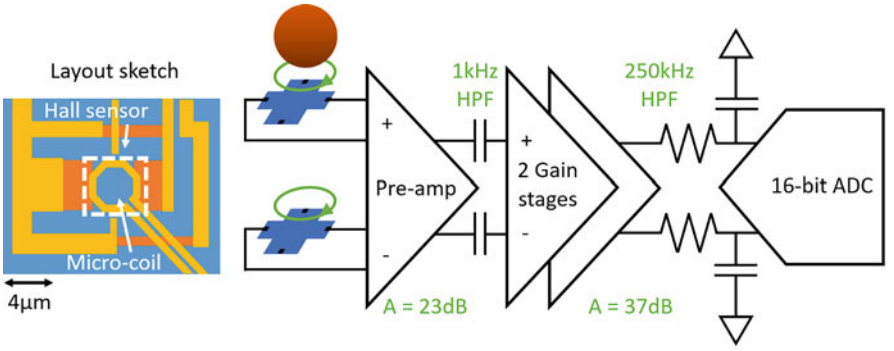

Fig. 22 Coil/Hall sensor layout and bead detection circuits (Based on [36])

of dendritic amplification of the tiny antibody-antigen proteins. Figure 22 shows its differential sensor operation method, the coil/hall-sensor layout, and bead-detection circuits.

This integrated CMOS biochip solution did not reach clinical trials and commercialization. Spun-out as Silicon Bio-Devices Inc., it received various grants and published results of some blood-analysis assays. It was rebranded as XipDx in 2018 but was reported as "out of business" in 2022 [37]. This could be due to simple statistics: most high-risk startups fail. This authors' view is that nonstandard CMOS process modifications (often in a research laboratory) can present obstacles to investment, to foundry selection, and to production scalability. Also, the choice of ELISA/immunoassay demonstrators pits it against the "cheap-and-cheerful" ELISA lateral-flow test strips, making clinical and market differentiation of this CMOS implementation more difficult.

4.4 CMOS Capacitive DNA Biosensor

At ISSCC 2012, Lee et al. [38] demonstrated capacitive DNA detection integrated on a CMOS process, with a limit of detection of 100 pmol, similar to Berney's discrete capacitive sensor of Fig. 14. Lee modified the CMOS process to integrate gold electrodes. The device locates two electrodes in a single current source as shown in Fig. 23. Oligomer DNA probes, complementary to the target DNA, are immobilized on the gold electrode surfaces.

The detection principle is the same as in Fig. 14, in which C_{dl} reduces when a target DNA binds or hybridizes to the capture probe on one electrode. This CMOS capacitive sensor is titled "Label-free DNA detection," meaning that no labels (fluorescent) are attached to the oligomer probes, unlike as in PCR. This simplifies the oligomer assay, while transferring the sensitivity challenge to the CMOS

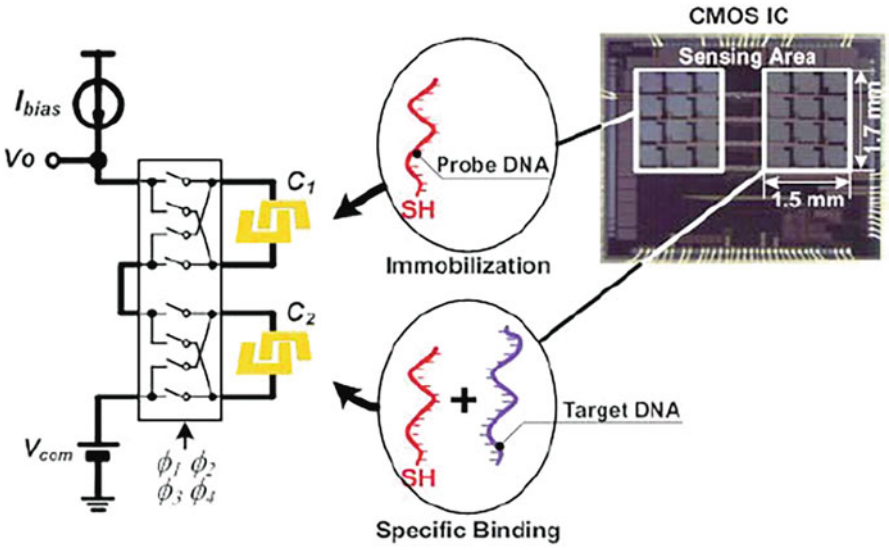

Fig. 23 CMOS capacitive DNA biosensor (From [38])

domain. In the differential architecture, the device detects the relative difference in the capacitance (ΔC,$|C_1$-$C_2|$) between a bare probe-functionalized working electrode and a hybridized working electrode. This difference is accumulated by a switched-capacitor-type parasitic-insensitive discrete-time integrator, which increases the signal-to-noise ratio (SNR) of the device significantly.

It is unclear if this CMOS chip has been commercialized. Its authors are currently focused on non-CMOS nanoplasmonic PCR microfluidic methods.

4.5 CMOS Bioluminescence Assay Sensor

At ISSCC 2017, Hassibi et al. (Insilixa) demonstrated bioluminescent DNA detection integrated on a CMOS process, as shown in Fig. 24 [39]. A limit of detection of target DNA in a sample is not given, since this architecture is detecting the billions of PCR amplicons from an upstream PCR reaction.

The CMOS process is modified by integrating an array of photodiodes, and long-pass multi-dielectric (TiO_2 and SiO_2) optical interference filters on the chip surface Multiple capture probes are designed to target different portions and mutations of the target DNA. The probes are then spotted onto individual sensors of the array. Amplicons from an upstream PCR reaction are applied to the sensor. The sensors with a positive optical signal then indicate which mutations are captured and detected. A high-dynamic-range photosensor detects small signals in the presence of a large background, with a unipolar $\Delta\Sigma$ photo-sensor circuit and capacitive transimpedance amplifier (CTIA) in each pixel integrate the photocurrent.

At VLSI 2021, Hassibi expanded the array to 1024 pixels [40]. This enabled simultaneous detection of many genetic mutations in the sample, important for

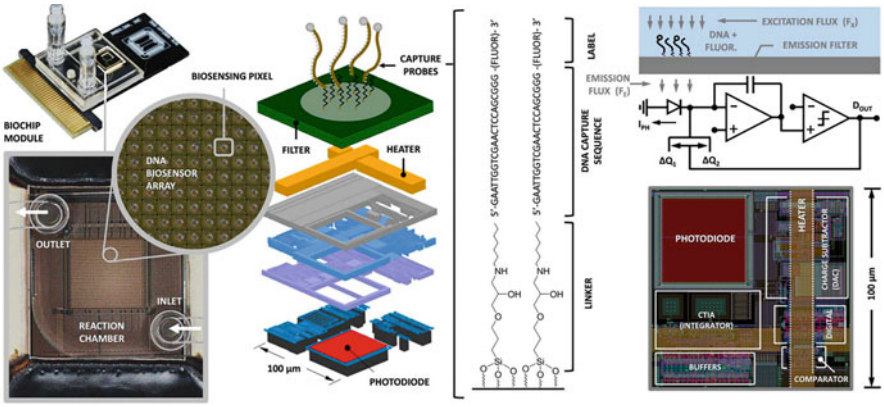

Fig. 24 (L): CMOS bio-luminescence sensor chip; (R): One photodiode pixel cell and photocurrent detection circuits (From [39])

medical diagnostic applications in variant tracking and antibiotic resistance. The technology was acquired by a large diagnostics company in 2021 [41].

5 The PNA-BeadCAP® Molecular Detection Assay

We developed the PNA-BeadCAP® nonenzymatic assay to simplify molecular detection of DNA and RNA targets. It employs synthetic peptide nucleic acid (PNA) probes, a novel bead-based assay, and capacitive detection of the beads with a standard-CMOS chip. The reader is referred to patents [42, 43, 44] for a description of the assay architecture and operating principles. Briefly, the sequential, highly specific in-solution hybridization events in the assay result in the release of a synthetic proxy bead over the biosensor. Subsequent capture of the proxy on the correct complementary biosensor leads to the transduction of the proxy presence into a capacitance signal, representing the amount of RNA in the sample.

5.1 PNA Probes

The PNA probes of the assay are synthesized by solid-phase FMOC peptide synthesis [45] and contain the standard A, T, C, and G monomer bases as in PCR DNA oligomer probes. However, whereas DNA probes have a negative charge due to their (deoxy)ribose-phosphate backbone, PNAs have a neutral backbone, due to substitution of N-(2-aminoethyl) -glycine units linked by amide bonds (Fig. 25):

This gives PNA probes many distinct advantages in a molecular assay:

PNA probe features	Advantages
Neutral backbone	Hybridize in any pH, in any crude sample ➔ eliminates sample-prep; the probes can capture RNA directly in whole blood or saliva
Very high specificity	High binding strength. Excellent single-base-mismatch (SBM or SNP) detection
Short (10–15 nt typically)	Can target more viruses and narrower regions (than PCR/LAMP probes of >25 nt typically). See PNA-probe illustrative example in Fig. 7
Higher melt temperature (tm) (10 °C–15 °C)	Stronger affinity than DNA/RNA sequences of same length. Better for Single Base Mismatch (SBM) & SNP detection, e.g., COVID-19 variants
Synthetic	Stable. Synthetic. No refrigeration. Minimal degradation/inhibition issues. Long shelf life
Bioorthogonal-PNA's	Synthetic. An abiotic replacement for the Biotin-Streptavidin linkers of other assays

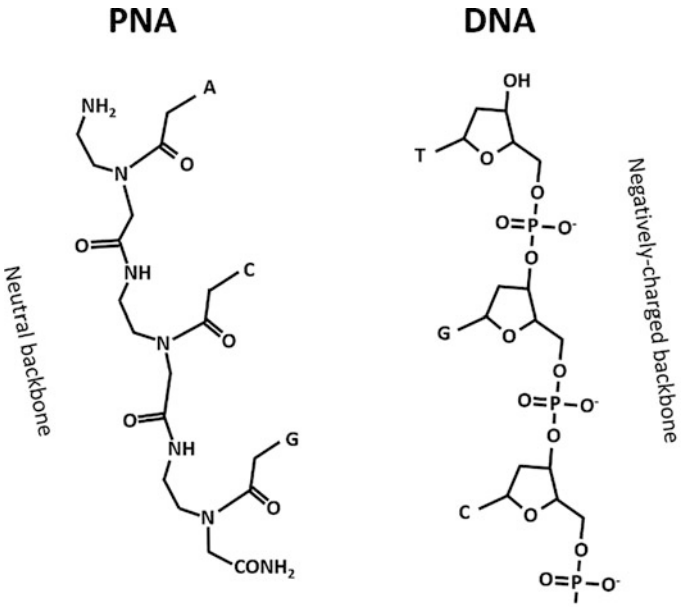

Fig. 25 PNA (neutral backbone) vs DNA (negatively charged backbone) structural differences (Based on [46])

5.2 BeadCAP® Capacitance Detection Method and Circuits

The beads from the upstream assay are detected and counted by capacitive sensing, in the fringe-field of interdigitated electrodes (IDE) fabricated in the CMOS top-metal layer, which are protected beneath the silicon nitride passivation layer (Fig. 26), that is, there is no contact between the assay biology and electronics. This removes corrosion risks and a potent source of interference. While most electric field lines are contained in the silicon, a small fringe portion of field lines protrude above the silicon nitride (Si_3N_4) passivation. These are the transducer portion, providing up to 100 mV electric field across a bead. This causes a dipole response in the bead, which correspondingly increases the charge on the electrodes, thereby increasing the capacitance as seen by the capacitive-to-digital converter.

The overall end-to-end assay performance (in vitro) is shown in Fig. 27 for three different concentrations of RNA spiked in biological samples. The top SEM photo shows beads correctly captured on the target sensor, spotted with a complementary PNA probe. The bottom photo shows no beads are captured for an off-target RNA. The limit of detection of this in vitro manual implementation of the assay is approximately 10 fmol. This is four orders of magnitude superior to the 100 pmol observed with the prior-art capacitive DNA sensors of Figs. 14 and 23.

Further work is underway to reduce the LOD to attomolar levels by assay miniaturization into a hand-held cartridge, automation, and other optimization steps

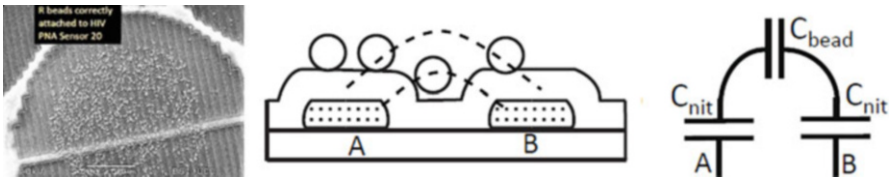

Fig. 26 Beads on chip surface and bead capacitance fringe-field sensing method

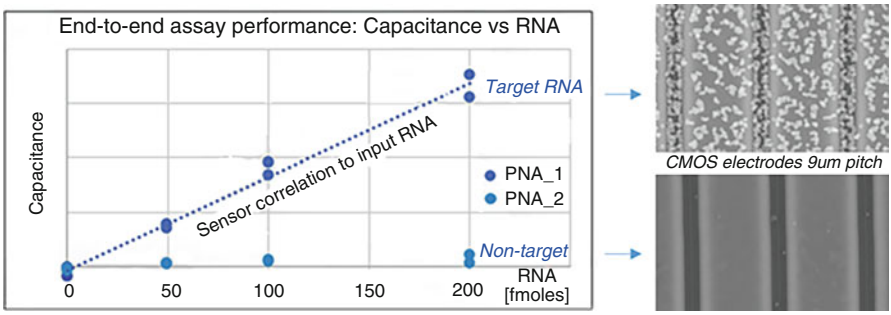

Fig. 27 Digital capacitance readout of RNA amount in lab biological samples

Fig. 28 Respiratory product profile of the miniaturized assay

[47]. The present sensor chip has 30 sensors, which enables multiplex detection of many sequences and variants in the target sample.

The target product profile for the fully integrated assay is shown in Fig. 28.

Resolving atto-Farad bead capacitances is key to the operation of this assay. Figure 29 shows simulations of the electric field around two electrodes, (L) in free space, and (R) with a ground-plane just beneath, the latter being representative of

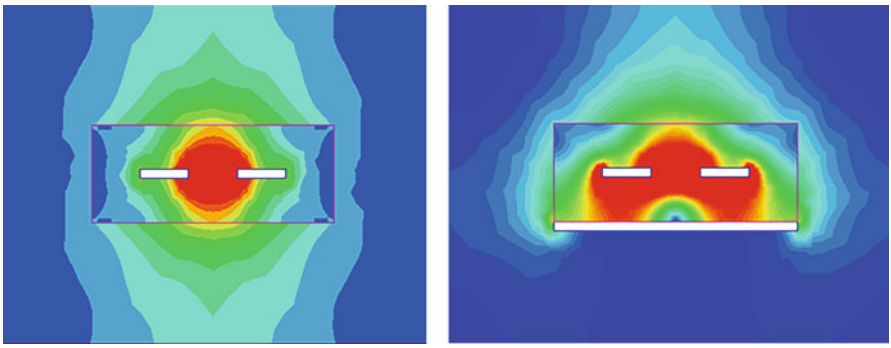

Fig. 29 Maxwell 2D electrostatic simulation of the field around two electrodes, (L) in free space and (R) with a nearby ground plane (red = 1 V/μm)

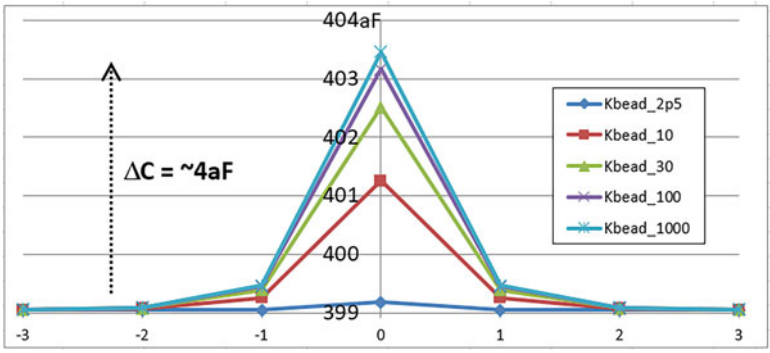

Fig. 30 Maxwell COMSOL Boundary Element Model (BEM) simulations of atto-Farad bead capacitance. At 1.6 V electrode voltage, 4aF equates to ~40 electrons

electrodes on a CMOS chip. Simulations like these are important to optimize the shape and dimensions of electrodes, to maximize the electric field to interrogate the magnetic or nonmagnetic nearby bead or particle on the chip surface.

Figure 30 shows electrostatic simulations of a single bead passing through the electrode electric field [48]. The resulting capacitance is 2aF to 4aF, depending on the dielectric constant K of the bead, for K ranging from 10 to 1000:

Figure 31 shows the architecture of the Candy second order ΣΔ converter for detecting the bead capacitance, and Fig. 32 shows the detailed modulator circuit implementation [49]. In this architecture, the IDE bead-sensing capacitor C_s (circled) is the input variable. The same reference voltage is applied to both the reference capacitor, C_{ref}, and the sensing capacitor C_s. This significantly reduces the effect of any reference noise. It also eliminates the requirement to calibrate or use any curvature correction within the on-chip bandgap voltage reference. Note the first integrator utilizes a fully floating input structure, with the input common mode to the amplifier being set by the feedback DAC. As the applied voltages to the

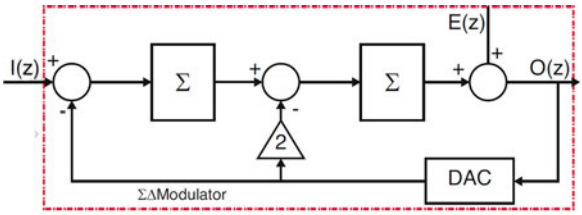

Fig. 31 Architecture of the sigma delta Σ Δ converter

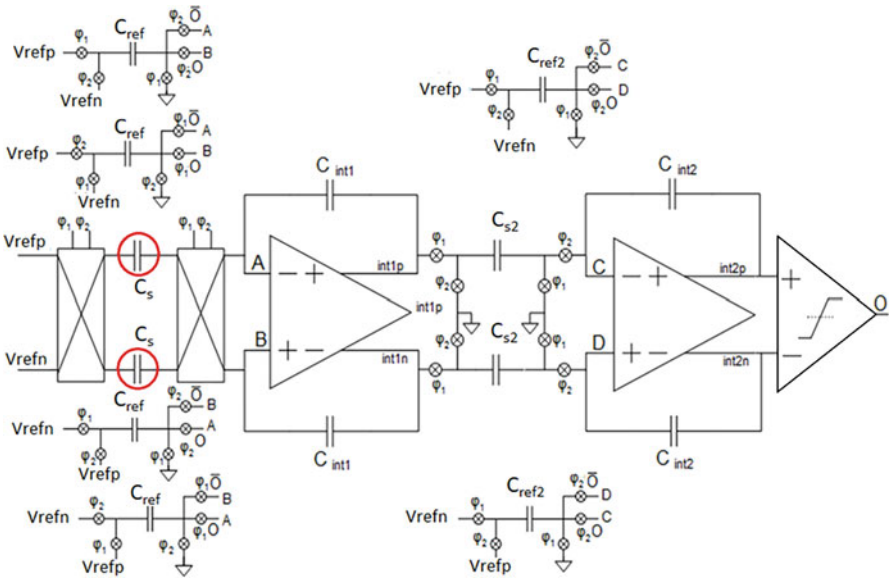

Fig. 32 Σ Δ modulator schematic

reference and sensor capacitors are the same, it is necessary to consider the thermal noise charge when examining the repeatability of the system.

The sampled thermal noise, Q_n, is correlated and is given by:

$$Q_n = CV_n = \sqrt{\mathrm{kTC}}$$

and the sampled thermal noise of the 1st integrator is:

$$Q_n = \sqrt{\mathrm{kT}\left(16.C_S + 8.C_{ref}\right)},$$

where T is temperature, k is Boltzmann's constant and C is the unit capacitance.

6 Discussion and Conclusions

In this chapter, we reviewed several different molecular detection methods and presented some biosensor and CMOS biochip detection examples. As Hassibi noted [1], it is a mixed picture of some commercial successes and many noncommercialized solutions. The ISFET and the wearable glucose sensor have reached

commercial success and widescale adoption, although this took decades. Reasons for noncommercialized examples are many and varied: difficulty in finding ongoing grant support or investments, especially for capital-intensive CMOS developments; difficulty in manufacturing (of coils, nano-rods, nanotubes), miniaturization negated by the need for large external components (GMR biosensor and magnets), incorrect product definition, and mismatch of biosensor technology to market application (e.g., CMOS immunoassay with unclear advantage versus incumbent lateral-flow immunoassay strip tests). Regulatory delays and inertia in the medical and clinical communities must also be factored in. These communities tend to be careful and conservative in adopting new technologies. CMOS process modifications (etching, nonstandard layers, or post-processing) may also be a factor, limiting foundry choice, affecting investment decisions (risk of process obsolescence), and future high-volume/low-cost scalability.

We have presented a nonenzymatic assay "PNA-BeadCAP," which aims to avoid many of these complexities. It employs synthetic PNA probes and a standard unmodified CMOS foundry process for the capacitive-sensor bead detector. There are no CMOS process modifications, which reduces cost and facilitates a wide choice of foundries. This is important for high-volume production scalability. Being fully synthetic and having no enzymes or fluorescent labels, the assay eliminates the need for cold-chain shipping and refrigeration. This will facilitate storage or operation at temperatures up to 40 °C and theoretically unlimited shelf-life, enabling volume building and stockpiling of tests for any future potential emergencies. PNA probes give higher specificity than PCR probes. The CMOS detector chip has 30 sensors, which will enable multiplexing and genotyping/variant-identification in this portable test. The in vitro assay has an LOD of 10 fmol, several orders of magnitude superior to previous capacitive DNA sensors. Work is now underway to reduce this to attomolar levels to approach PCR sensitivity levels, by assay optimization, automation, and miniaturization to a hand-held kit format, intended for home use and self-testing of respiratory viruses from a self-sampled saliva sample.

References

1. S. Swaminathan, P. Bento, et al., *Consolidated Telemedicine Implementation Guide* (World Health Organization, Geneva, 2022) WHO https://www.who.int/publications/i/item/9789240059184. Retrieved 9 Jan 2023
2. A. Hassibi, *CMOS Biochips: The Good, the Bad, and the Hype* (TWEPP Workshop 14 Sep 2018). https://indico.cern.ch/event/608587/contributions/2704610/attachments/1523865/2381946/Hassibi_TWEPP_2017_final_v2.pdf. Retrieved 5 Dec 2022
3. B. O'Farrell, *Evolution in Lateral Flow-Based Immunoassay Systems* (Springer, Lateral flow immunoassay, 2009), pp. 1–33
4. B.E. Slatko et al., Overview of next-generation sequencing technologies. Curr. Protoc. Mol. Biol. **122**(1), e59 (2018). https://doi.org/10.1002/cpmb.59. PMID: 29851291; PMCID: PMC6020069
5. L.G. Gordon et al., Estimating the costs of genomic sequencing in cancer control. BMC Health Srv. Res. **20**, 492 (2020). https://doi.org/10.1186/s12913-020-05318-y

6. F. Wu et al., A new coronavirus associated with human respiratory disease in China. Nature **579**(7798), 265–269 (2020). https://doi.org/10.1038/s41586-020-2008-3. Epub 2020 Feb 3. Erratum in: Nature. 2020 Apr;580(7803):E7. PMID: 32015508; PMCID: PMC7094943
7. V. Corman et al., Detection of 2019 novel coronavirus (2019-nCoV) by real-time RT-PCR. Eur. Secur. **25**, 2000045 (2020). https://doi.org/10.2807/1560-7917.ES.2020.25.3.2000045
8. A. Hassibi, *Mass-deployable Molecular Diagnostics (MDx), including COVID-19 Testing: An IC Designer's Perspective* (Keynote at Annual TxACE Symposium, October 19, 2020)
9. T. Brock, H. Freeze, Thermus aquaticus gen.n. and sp.n., a nonsporulating extreme thermophile. J. Bacteriol. **98**(1), 289–297 (1969). https://doi.org/10.1128/jb.98.1.289-297.1969. PMID: 5781580; PMCID: PMC249935
10. Skytrax, London, UK, "*The varying costs of a PCR test at airports around the world*",https://skytraxratings.com/the-varying-costs-of-a-pcr-test-at-airports-around-the-world. Retrieved 5 Dec 2022
11. FIND-Dx, *Negotiated Prices, GeneXpert II R2 $9920*, https://www.finddx.org/pricing/genexpert/. Retrieved 5 Dec 2022
12. FDA Emergency Use Authorization EUA203089, *Visby Medical COVID-19 Point of Care Test*, https://www.fda.gov/media/145914/download. Retrieved 5 Dec 2022
13. B. Andreyev, et al., *Devices and Methods for Molecular Diagnostic Testing*, (US patent application US, 2016/0186240, June 30, 2016)
14. A. Renzoni et al., Analytical evaluation of Visby medical RT-PCR portable device for rapid detection of SARS-CoV-2. *Diagnostics**11***, 813 (2021). https://doi.org/10.3390/diagnostics11050813
15. *Visby Medical 10-pack tests $1550,*https://www.meenta.io/product/visby-rapid-covid-19-pcr-test-power-cord-2/. Accessed 12 Mar 2022
16. D. Thompson and Yu Lei, "Recent progress in RT-LAMP enabled COVID-19 detection", Mini review:, Sensors and Actuators Reports, Volume 2, Issue 1, 2020, 100017., ISSN 2666-0539, https://doi.org/10.1016/j.snr.2020.100017
17. T. O'Leary et al., Sensitivity of ID NOW and RT-PCR for detection of SARS-CoV-2 in an ambulatory population. elife **20**(10), e65726 (2021). https://doi.org/10.7554/eLife.65726. PMID: 33876726; PMCID: PMC8081522
18. FDA Emergency Use Authorization E210180, *Cue COVID-19 Test for Home and Over The Counter (OTC) Use*, https://www.fda.gov/media/146467/download. Retrieved 5 Dec 2022
19. Cue Health price list, https://shop.cuehealth.com/. Retrieved 5 Dec 2022
20. Cue Health, *Cue COVID-19 Test: Instructions for Use*, https://www.fda.gov/media/138826/download. Retrieved 5 Dec 2022
21. KM Lei et al, CMOS biosensors for in vitro diagnosis – Transducing mechanisms and application https://doi.org/10.1039/C6LC01002D (Critical Review) Lab Chip, 2016, **16**, 3664–3681
22. K. Kramp, *How to Hack a Glucose Sensor*, https://towardsdatascience.com/how-to-hack-a-glucose-sensor-ebaaf2238170. Retrieved 5 Dec 2022
23. J. Barton et al., Long-range photoinduced electron transfer through a DNA helix. Science **262**(5136), 1025–1029 (1993). https://doi.org/10.1126/science.7802858
24. C. Berggren et al., A feasibility study of a capacitive biosensor for direct detection of DNA hybridization. J. Electroanalysis **11**(3), 156–160 (1999)
25. H. Berney et al., A DNA diagnostic biosensor: Development, characterisation and performance. Sensors Actuators B Chem. **68**(1–3), 100–108., ISSN 0925-4005, (2000). https://doi.org/10.1016/S0925-4005(00)00468-8
26. D.R. Baselt et al., A biosensor based on magnetoresistance technology. Biosens. Bioelectron. **13**(7–8), 731–739 (1998). https://doi.org/10.1016/s0956-5663(98)00037-2. PMID: 9828367
27. R. Widlar, Some circuit design techniques for linear integrated circuits. IEEE Trans. Circuit Theory **12**(4), 586–590 (1965). https://doi.org/10.1109/TCT.1965.1082512
28. P. Bergveld, Development of an ion-sensitive solid-state device for neurophysiological measurements. I.E.E.E. Trans. Biomed. Eng. **BME-17**(1), 70–71 (1970). https://doi.org/10.1109/TBME.1970.4502688

29. P. Bergveld, Thirty years of ISFETOLOGY: What happened in the past 30 years and what may happen in the next 30 years. Sens. Actuators B Chem. **88**(1), 1–20., ISSN 0925-4005, (2003). https://doi.org/10.1016/S0925-4005(02)00301-5
30. J. Bausells et al., Ion-sensitive field-effect transistors fabricated in a commercial CMOS technology. Sens. Actuators B Chem. **57**(1–3), 56–62., ISSN 0925-4005, (1999). https://doi.org/10.1016/S0925-4005(99)00135-5
31. C. Toumazou et al., *A sensing circuit utilising an ion sensitive field effect transistor*, GB patent 2416210B
32. D.M. Garner et al., A multichannel DNA SoC for rapid point-of-care gene detection, in *2010 IEEE International Solid-State Circuits Conference-(ISSCC)*, (IEEE, 2010, San Francisco), pp. 492–493. https://doi.org/10.1109/ISSCC.2010.5433834
33. A. Hassibi and N. Pourmand, *Transient Electrical Signal Based Methods and Devices for Characterizing Molecular Interaction and/or Motion in a Sample*, US patent 722,3540, May 29 2007
34. J. Rothberg et al., An integrated semiconductor device enabling non-optical genome sequencing. Nature **475**, 348–352 (2011). https://doi.org/10.1038/nature10242
35. X. Huang, et al., A dual-mode large-arrayed CMOS ISFET sensor for accurate and high-throughput pH sensing in biomedical diagnosis, IEEE Trans. Biomed. Eng., Vol. 62, No. 9, Sep. 2015, pp. 2224–2233
36. O. Florescu, *Fully Integrated Complementary Metal Oxide Semiconductor (CMOS) Bio-Assay Platform*. https://www.researchgate.net/publication/267705427_Fully_Integrated_Complementary_Metal_Oxide_Semiconductor_CMOS_Bio-Assay_Platform. Retrieved 5 Dec 2022
37. Pitchbook https://pitchbook.com/profiles/company/123267-16. Retrieved 5 Dec 2022
38. K.-H. Lee et al., CMOS capacitive biosensor with enhanced sensitivity for label-free DNA detection. *IEEE Int. Solid State Circuits Conf.***2012**, 120–122 (*2012*). https://doi.org/10.1109/ISSCC.2012.6176945
39. A. Hassibi et al., A fully integrated CMOS fluorescence biochip for multiplex polymerase chain-reaction (PCR) processes, in *2017 IEEE International Solid-State Circuits Conference (ISSCC)*, (IEEE, San Francisco, 2017), pp. 68–69. https://doi.org/10.1109/ISSCC.2017.7870264
40. A. Manickam et al., Multiplex PCR CMOS biochip for detection of upper respiratory pathogens including SARS-CoV-2. *Symposium on VLSI Circuits***2021**, 1–2 (*2021*). https://doi.org/10.23919/VLSICircuits52068.2021.9492353
41. https://www.linkedin.com/in/arjang. Retrieved 5 Dec 2022
42. B. O'Farrell, T. Cummins, *Sample Preparation Method and Apparatus*, US patent 10,160,966
43. B. O'Farrell and T. Cummins, *Nucleic Acid Analysis Method and Apparatus*, US patent 10,738,348
44. T. Cummins, B. O'Farrell, *Capacitive Sensor and Method of Use*, US patent 10,746,683
45. K. Oshaben, C. O'Connell, D. Appella, et al, *RNA target enrichment or depletion of biological samples,* USPTO patent-pending application 2021/0277387
46. A. Ray and B Norden, "Peptide nucleic acid (PNA): Its medical and biotechnical applications and promise for the future", FASEB J., Vol 14, Is 9, https://doi.org/10.1096/fasebj.14.9.1041
47. M. McCarthy, P. Free, J. O'Driscoll, J. Walshe, C. O'Sullivan, et al, *Diagnostic Device and System*, US patent 11,459,601
48. T. Dalton, D. McGuire, et al, *Single-Bead Capacitive Detector for Microbiological Applications*, USPTO patent-pending application 63/304,312
49. I. O'Connell et al, *$\Sigma\Delta$ A-to-D Converter for Use in Sensing Applications* (IEEJ Int'l Analog VLSI Workshop, 2007)